Pharm Res (2011) 28:472–479
DOI 10.1007/s11095-010-0296-2

PERSPECTIVE

Convection and Retro-Convection Enhanced Delivery: Some Theoretical Considerations Related to Drug Targeting

J. P. Michael Motion • Grace H. Huynh • Francis C. Szoka Jr. • Ronald A. Siegel

Received: 2 August 2010 / Accepted: 28 September 2010 / Published online: 21 October 2010

ABSTRACT Delivery of drugs and macromolecules into the brain is a challenging problem, due in part to the blood–brain barrier. In this article, we focus on the possibilities and limitations of two infusion techniques devised to bypass the blood–brain barrier: convection enhanced delivery (CED) and retro-convection enhanced delivery (R-CED). CED infuses fluid directly into the interstitial space of brain or tumor, whereas R-CED removes fluid from the interstitial space, which results in the transfer of drugs from the vascular compartment into the brain or tumor. Both techniques have shown promising results for the delivery of drugs into large volumes of tissue. Theoretical approaches of varying complexity have been developed to better understand and predict brain interstitial pressures and drug distribution for these techniques. These theoretical models of flow and diffusion can only be solved explicitly in simple geometries, and spherical symmetry is usually assumed for CED, while axial symmetry has been assumed for R-CED. This perspective summarizes features of these models and provides physical arguments and numerical simulations to support the notion that spherical symmetry is a reasonable approximation for modeling CED and R-CED. We also explore the potential of multi-catheter arrays for delivering and compartmentalizing drugs using CED and R-CED.

KEY WORDS blood brain barrier · convection enhanced delivery · finite element analysis · mathematical model · retro-convection enhanced delivery

J. P. M. Motion · G. H. Huynh · F. C. Szoka Jr.
Joint Graduate Group in Bioengineering
University of California at San Francisco and Berkeley
San Francisco, California 94143-0446, USA

F. C. Szoka Jr.
Departments of Bioengineering
Therapeutic Sciences and Pharmaceutical Chemistry
University of California
San Francisco, California 94143-0912, USA

R. A. Siegel
Department of Pharmaceutics and Biomedical Engineering
University of Minnesota
Minneapolis, Minnesota 55455, USA

R. A. Siegel (✉)
Department of Pharmaceutics 9-177 WDH, University of Minnesota
308 Harvard St. S.E.
Minneapolis, Minnesota 55455, USA
e-mail: siege017@umn.edu

F. C. Szoka Jr. (✉)
University of California at San Francisco
513 Parnassus Ave HSE 1145
San Francisco, California 94143-0446, USA
e-mail: szoka@cgl.ucsf.edu

ABBREVIATIONS

CED	convection enhanced delivery
ECF	extracellular eluid
i.c.	intracranial
ISF	interstitial fluid
PDE	partial differential equation
R-CED	retro-convection enhanced delivery
s.c.	subcutaneous

INTRODUCTION

Primary malignant brain tumors are a significant therapeutic challenge in spite of substantial advances in tumor imaging, neurosurgery, and radiation therapy. The efficacy of potent chemotherapy drugs is limited by biochemical and physiological barriers, including poor drug delivery to

the brain tumor mass and its peripheral regions (1–3), rapid clearance from the brain extracellular space (4), high intratumor pressure (5) and toxicity to normal brain tissue. More effective patterning of fluid movement through the tumor or diversion of fluid from entering normal brain parenchyma could improve brain tumor therapy.

Over the past decade, convection enhanced delivery (CED), employing a positive pressure infusion directly into the brain, has shown promising results in both animal models and clinical trials (6–9). CED distributes macromolecules, proteins, and particulate therapies into large volumes of tissue (10–12). Retro-convection enhanced delivery (R-CED), which removes interstitial fluid through a microdialysis catheter (13), has also been introduced to deliver drugs into brain tumors (14). Continuous flow of a hyperosmotic high molecular weight polymer solution, as the dialysate, drives fluid flow from the interstitial space into the catheter, lowering interstitial pressure and leading to convective flow of fluid, including drug, from capillaries into tissue. By themselves or in combination, CED and R-CED provide tools to pattern interstitial flow in the brain. Fig. 1 illustrates CED and R-CED.

Theoretical approaches of varying complexity, ranging from analytical to finite element models, have been developed to better understand and predict the interstitial distribution of material infused by CED (15–20). These models have also been used to predict features such as the interstitial fluid pressure, interstitial fluid velocity, tissue swelling, and transvascular fluid exchange rate during CED. Although these models do not recapitulate all aspects of fluid distribution in the brain following CED, they are instructive regarding what might be achieved in fluid patterning by a multi-catheter infusion protocol.

Recently, Wang and Olbricht published an analysis of R-CED driven by hydrostatic or osmotic flow across a tubular microdialysis membrane (21). It was shown that drug concentration near the catheter is enhanced when it cannot permeate through the membrane, but such enhancement is marginal when drug is permeable or semipermeable in the membrane. Removal of drug into the catheter largely defeats the purpose of R-CED, which is to draw drug into brain or tumor tissue from the capillaries.

Analytical models of flow and diffusion for both CED and R-CED can only be solved explicitly in simple geometries, and spherical symmetry is usually assumed for CED, while axial symmetry was assumed by Wang and Olbricht for R-CED (21). Although real systems are more complicated, in this article we provide physical arguments and supporting numerical studies indicating that spherical symmetry is a reasonable approximation in both CED and R-CED. We also explore the potential benefits of fluid delivery through multiple catheters. For example, drug-free fluid flow out of one catheter can be used to divert drug-containing fluid delivered from another catheter, offering protection to tissue surrounding the first catheter. Thus, drug delivered near the tumor/tissue interface might, in principle, be localized on the tumor side, with a nonspherical, nonsymmetric distribution. This idea is illustrated with a simple phantom construct.

FLUID FLOW MODELING

Fluid Balance Equations

Following previous analyses, we utilize a simplified modeling approach in which fluid flow through tissue is described by Darcy's law,

$$\overline{u} = -K\nabla p \tag{1}$$

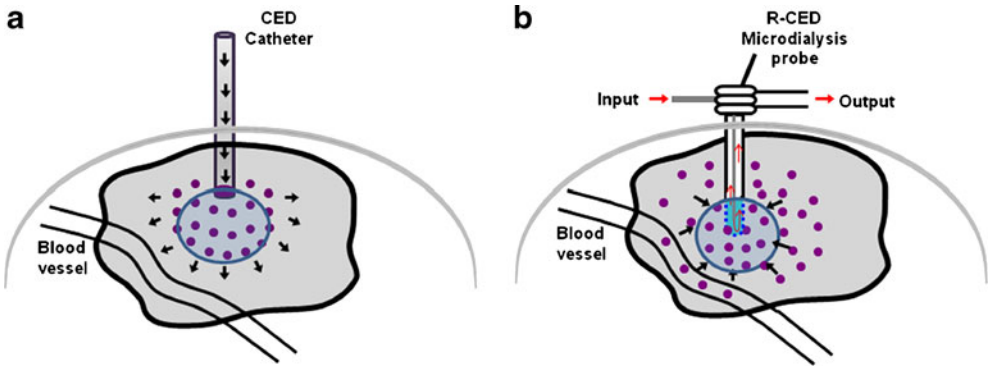

Fig. 1 Schematic illustration of fluid movement in the brain under the influence of CED or R-CED. **a** A CED catheter is implanted into the brain, and a solution is perfused under a positive pressure (*black arrows*). The therapeutic solution convects in response to the pressure field. This allows permeation and distribution of the therapeutic agent contained in the solution into the region of interest. **b** To remove fluid from the brain, a hyperosmotic solution is perfused into the brain using a microdialysis probe. The microdialysis membrane separates the hyperosmotic perfusate from the brain interstitial. Fluid then flows from the blood into the ISF and towards the microdialysis probe as diagrammed with the black arrows. The fluid then exits through the output tube of the probe.

and the equation for continuity of the fluid,

$$-\varphi\nabla \bullet \overline{u} - \varphi L_{pc} s(p - p_e) = 0 \tag{2}$$

where p is interstitial hydraulic pressure at a given location, $\overline{u}$ is local (vector) fluid velocity, p_e is effective or Starling pressure of the capillary bed calculated according to Starling's law ($p_e = p_c + \sigma(\pi - \pi_c)$, where p_c and p_c and the intercapillary hydraulic and osmotic pressures, p is the interstitial osmotic pressure, and s is the reflection coefficient of the capillary wall), φ is volume fraction of tissue available for interstitial flow, s is capillary surface area per unit volume of tissue, K is hydraulic conductivity of interstitial space, and L_{pc} is the filtration coefficient of the capillary walls.

The parameters p_e, φ, s, k, and L_{pc} are all assumed to be constant for a given tissue (e.g. brain parenchyma, tumor). The velocity vector $\overline{u}$ is taken as a volume averaged field variable, with volume averaging effects introduced at the level of the Darcy coefficient, K. Combining Eqs. 1 and 2 obtains the equation for the difference between interstitial and effective, Starling capillary pressure, $\widetilde{p} = p - p_e$

$$\nabla^2\widetilde{p} = \kappa^2\widetilde{p} \tag{3}$$

where $\kappa = \sqrt{L_{pc}s/K}$ has units of inverse distance.

Equation 3 is of the Helmholtz type. In the absence of fluid exchange between tissue and capillaries (L_{pc}=0) it reduces to Laplace's equation, $\nabla^2\widetilde{p} = 0$. More detailed treatments also consider drug transport by diffusion and exchange across capillary walls. Since our present interest is fluid flow, these contributions to drug transport will not be considered here.

CED and R-CED from a Spherically Symmetric Catheter Tip

To denote the flow of drug solution through an idealized spherically symmetric CED catheter tip of radius R_m and centered at the origin by Q, using spherical coordinates to represent position, i.e. $r = (x, y, z)$, $|r| = \sqrt{x^2 + y^2 + z^2}$, $\overline{i}_r = r/|r|$, the velocity field around the source will be $\overline{u} = u_r\overline{i}$, $r > R_m$. Equations 3 and 1 become, respectively,

$$\frac{\partial^2\widetilde{p}}{\partial r^2} + \frac{2}{r}\frac{\partial\widetilde{p}}{\partial r} = \kappa^2\widetilde{p} \qquad r > R_m \tag{4}$$

$$u_r = -K\frac{\partial\widetilde{p}}{\partial r} \qquad r > R_m \tag{5}$$

Fluid flow continuity at the tip/tissue interface prescribes the boundary condition

$$Q = 4\pi R_m^2\varphi u_r(R_m) = -4\pi R_m^2\phi K\left.\frac{\partial\widetilde{p}}{\partial r}\right|_{r=R_m} \tag{6}$$

Far from the tip, interstitial and capillary fluids are in Starling equilibrium, i.e.

$$\widetilde{p}(r) \to 0, \quad r \to \infty \tag{7}$$

The solution to Eqs. 4–7 is

$$\widetilde{p} = \left[\frac{Q}{4\pi\phi Kr}\right]\frac{e^{-\kappa(r-R_m)}}{1+\kappa R_m} \qquad r > R_m \tag{8}$$

$$u_r = \left[\frac{Q}{4\pi\phi r^2}\right]\left(\frac{1+\kappa r}{1+\kappa R_m}\right)e^{-\kappa(r-R_m)} \qquad r > R_m \tag{9}$$

The terms in the square brackets refer to pressure and flow that would occur in the absence of fluid exchange between tissue and capillaries, i.e. k=0, (Laplace equation solution). The remaining terms quantitate the relative effects of fluid exchange compared to interstitial flow. These terms rapidly decay to zero for $r \gg 1/k$ and limit the region of influence of flow from the catheter. The quantity $1/k$ is recognized as a "screening length" over which flow across capillary walls buffers perturbations in pressure due to infusion.

When tip radius is significantly smaller than the screening length, i.e. $\kappa R_m \ll 1$, Eqs. 8 and 9 simplify to $\widetilde{p} = q\kappa e^{-\kappa r}/4\pi\phi K(\kappa r)$ and $u_r = [q\kappa^2/4\pi\phi(\kappa r)^2](1+\kappa r)e^{-\kappa r}$, respectively, for $r > R_m$. In this case, pressure and velocity at a point beyond the tip surface decay according to the number of screening lengths the point lies away from the center of the tip.

To model R-CED, we must include the effects of the dialysis membrane, whose hydraulic permeability will be denoted by L_{pm}. We retain spherical symmetry in the model. We assume, as will be argued below, that this simplification will not lead to great error. Taking the intercapillary Starling pressure as the reference, and assuming that the osmolyte (e.g. high MW dextran) cannot permeate through the dialysis membrane but all other solutes can, the relevant pressure inside the catheter lumen is $\widetilde{p}_l = p_l - \pi_l - p_e$ where the subscript l refers to the lumen. For R-CED, this pressure will be negative. Flow continuity at the membrane/tissue interface warrants that

$$L_{pm}[\widetilde{p}_l - \widetilde{p}(R_m)] = -\varphi K\left.\frac{d\widetilde{p}}{dr}\right|_{r=R_m} \tag{10}$$

Replacing Eq. 6 with Eq. 11, the pressure and velocity fields surrounding a spherical R-CED catheter become

$$\begin{aligned}\widetilde{p} &= (1-\theta)\left(\frac{R_m}{r}\right)e^{-\kappa(r-R_m)}\widetilde{p}_l\,;\; u_r \\ &= (1-\theta)K\frac{R_m}{r^2}\left(\frac{1+\kappa r}{1+\kappa R_m}\right)e^{-\kappa(r-R_m)}\widetilde{p}_l \qquad (11)\\ r &> R_m\end{aligned}$$

where

$$\theta = \frac{1}{1+L_{pm}R_m/\varphi K(1+\kappa R_m)} \qquad (12)$$

is the fraction of Starling pressure that is dissipated in the membrane. The cases $\theta=0$ and $\theta=1$ correspond, respectively, to membrane and tissue control of R-CED flow. For $\kappa R_m \ll 1$, Eq. 11 simplifies to $\widetilde{p} = (1-\theta)(R_m/r)e^{-\kappa r}\widetilde{p}_l$, .

Nonspherical Catheter Tips

Having presented equations for the idealized geometry, we turn to the importance of precise tip geometry. For CED, delivery is through the open end of a narrow shaft. For R-CED, tubular microdialysis membranes are used, and Wang and Olbricht's work assumed cylindrical geometry. Calculations based on this assumption are strictly correct only for catheters with large axis-to-radius ratios or when looking at tissue that is very close to the catheter. We now argue that spherical symmetry often provides a useful and reasonably accurate approximation for CED and R-CED. This approximation is commonly used in the electrostatics of colloidal solutions, where the Helmholtz equation (linearized Poisson-Boltzmann equation) is prominent (22,23).

Let d be the largest length scale of the catheter tip, such as its radius or half its length. Also let the radial coordinate, r, be a suitably chosen centroid of the catheter tip. Then our assertion is, roughly, that spherical symmetry will apply for $r>d$, and Eqs. 8, 9 and 11 will be good approximations. For $r<d$, shape effects are more important.

To further support this assertion, several cases were studied in the COMSOL 3.5a simulation environment (COMSOL, Inc., Burlington MA), which solves partial differential equations (PDEs), subject to appropriate boundary conditions, using the finite element method. This method, despite its approximations, is preferred over analytic solutions. Even for the simple case of two ideal spherical catheters delivering fluid at the same rate, superposition does not provide a correct solution since each catheter's presence perturbs the flow pattern generated by the other catheter.

To solve PDEs in COMSOL, a finite domain corresponding to tissue is prescribed, as is the geometry of the catheter(s). The type of equation (usually Helmholtz in the present case) is then selected, and boundary conditions are prescribed at the catheter surfaces and at the edges of the domain. To minimize the effect of domain boundaries on the numerical solution, the domain should be large compared to catheter radius or length and distance between the catheter's tip. In the present simulations, Dirichlet conditions (zero Starling pressure, similar to Eq. 7) are prescribed at the domain boundary. Neumann conditions (pertaining to pressure gradients) are prescribed at catheter boundaries. Since we are only interested in patterns, no attempt has been made to introduce physiological parameters, flows magnitudes, or specific Starling pressures.

As a first example, Fig. 2a shows that a cubic tip, with fluid flowing uniformly and equally out of each face, is surrounded by an essentially spherical pressure field, except very close to the surface. Placed side by side with a

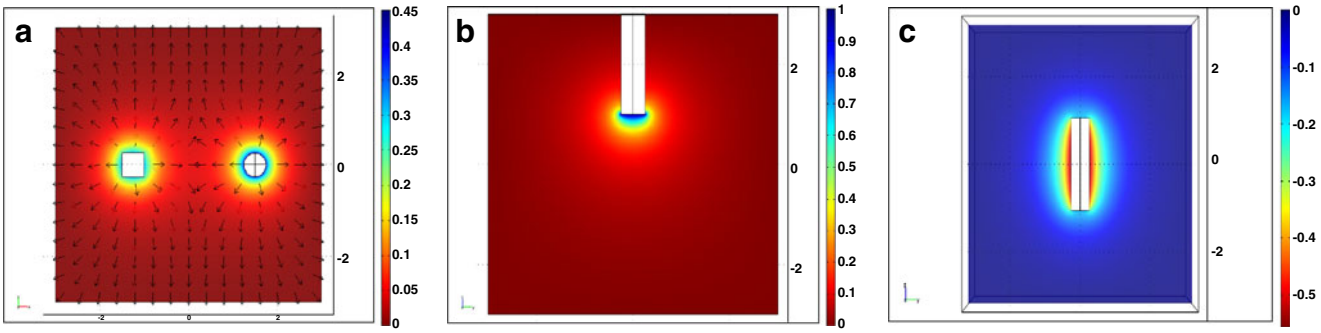

Fig. 2 Finite element analysis of R-CED. **a** Finite element analysis of spherical and cubic "model" catheter tips. We designed objects with equal diameter and set boundary conditions such that the flux emitting from the cube and the sphere are the same, and $kR_m=0.25$. Pressure variations are represented by color changes, and the arrows correspond to the direction of the velocity field with normalized magnitudes. **b** Finite element analysis of a CED catheter tip fed by unidirectional plug flow with $kR_m=0.5$. **c** Finite element analysis of R-CED Flow with $kR_m=0.5$ and $kd=4$. The shaft tips are to be impermeable, and the surrounding edges were modeled as model membranes. Relative pressures are mostly negative close to the membrane where reverse flow is being generated.

spherical tip with the two tips separated by a sufficient distance that their interaction is small, and with equal flow emerging from the two tips, the two objects produce essentially identical pressure and flow fields away from their surfaces, while fields near the surfaces depend on shape. Fig. 2b shows simulations of delivery from a shaft, with unidirectional flow to the lumen, which opens at its end into the tissue. The outer body of the shaft is impermeable to fluid flow. For simplicity, flow inside the shaft is modeled as plug instead of Poisseiulle flow. This figure demonstrates that a nearly spherically symmetric pressure/flow profile develops soon after fluid leaves the catheter tip, even though the tip itself is circular and shaft's wall blocks fluid flow. Intuitively, as one moves farther away from the tip, the surface area of the isobar becomes larger compared to the cross-sectional area of the shaft. The shaft therefore becomes much less important in "shaping" the front. Fig. 2c displays the flow pattern into a cylinder, representing R-CED into a microdialysis membrane. The axial/radial ratio is 8. Close to the membrane, the (negative) pressure contours are nearly cylindrical, but they round out as one moves away from the tube. With a smaller value of k (larger $1/k$), more such contours would be discernable.

Multiple Catheter Delivery

The previous sections show that catheter shape has little effect on pressure and flow profiles once fluid moves a sufficient distance from the catheter tip. We now consider the effects of flow from one catheter on flow from a second catheter. The simplest situation is two identical catheters placed at a distance from each other in a medium (tissue) with uniform properties. Such a system is physically modeled (see below) using an agarose gel phantom. Suppose that one catheter delivers drug, while the other delivers a drug-free, blank solution. If flows from the two catheters are equal, then the flows will collide at the "mirror" plane perpendicular to the two catheters and proceed along that plane. This phenomenon is illustrated by the flow arrows in Fig. 2a. Now suppose that flow from the "blank" catheter is stronger. Then, the fluids will collide along a surface that is closer to and bent around the drug-delivering catheter. If the former and latter catheters are properly placed inside and outside of the tumor, and flows are properly selected, based on the tissue properties of tumor and brain parenchyma (including differences in tissue permeability, capillary densities and filtration coefficients, and the absence of lymphatics in tumor, factors which give rise to increased interstitial pressure in tumor), it seems possible to focus drug delivery into the tumor and substantially reduce exposure in the parenchyma. Conversely, flow of a radioprotective agent from outside the tumor could be "steered away" from tumor tissue by flow of blank solution from a catheter inside the tumor.

A second possible dual probe configuration would involve convective drug delivery from one catheter and fluid removal by the other. Note that the latter catheter is not used in the same way as has been previously considered for R-CED, since drug is not being pulled out of the circulation through capillaries, but rather is supplied by the delivery catheter. In this case, flow is predicted from the delivery catheter to the removal catheter, with a pattern resembling the alignment of iron filings over two-pole magnet. For reasons already identified by Wang and Olbricht, this technique seems less promising than dual CED, since it is more difficult to pull osmotically than it is to push hydraulically, due to added hydraulic resistance from the microdialysis membrane and tradeoffs between osmotic pressure and viscosity of the dialysate (14), and since drug will be lost into the removal catheter, unless that catheter's membrane is impermeable to drug.

DUAL PROBE CED IN AN AGAROSE GEL PHANTOM

Dual probe CED experiments were carried out in an agarose gel phantom by adapting methods that have been described elsewhere for acute stereotactic infusion (10,24,25). Bankiewicz and colleagues (26) have used a similar system to visualize fluid distribution following single probe CED. Briefly, cannulae were prepared from fused silica tubing with an outer diameter of 0.16 mm (Polymicro Technologies, Phoenix, AZ), extending 1–2 mm from the tip of a 24 gauge needle used for support (26). Cannulae were inserted into the 0.5% agarose gel (UltraPure Agarose, 15510-019, Invitrogen, Carlsbad, CA), prepared immediately before use, approximately 8 mm below the surface of the gel, with tip outlets separated by 2 mm. An external syringe pump (Bioanalytical Systems Inc., West Lafayette, IN) was used to infuse solutions containing dyes (67 kD albumin-Alexa Fluor 647 in one cannula and 3 kD Texas Red-dextran in the other) at an increasing flow rate as follow 0.1 mL/min for 5 min, 0.2 mL/min for 5 min, 0.5 mL/min for 5 min, and 0.8 mL/min for 30 min for a total volume of 28 mL infused. Following the infusion, the probes were removed slowly over 1 min. Photographs were taken by slicing the agarose phantom and imaging on a Kodak Imagestation 4000. Alexa Fluor 647 was visualized individually using the 625 nm excitation filter and the 700 nm emission filter. Texas Red was visualized individually using the 535 nm excitation filter and the 600 nm emission filter.

Fig. 3a shows the optical image of the two probes, with Alexa Fluor in blue and Texas Red in red. Fluorescence

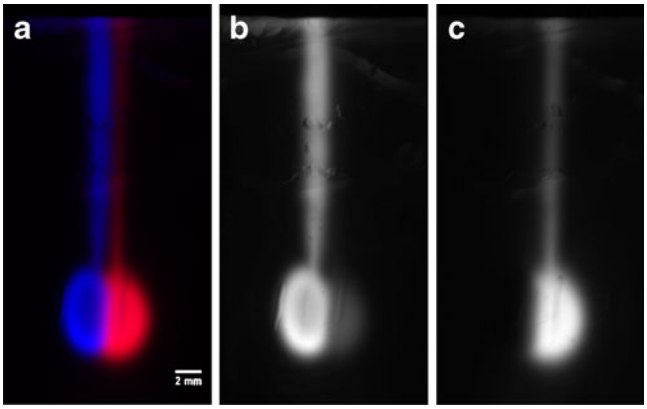

Fig. 3 Dual probe CED in an agarose gel phantom. **a** Dispersion of Alexa Fluor-albumin, MW 67 kD (*blue*) and Texas Red, MW 3 kD (*red*) into agarose gel following equal rate volumetric infusion though identical catheters, observed by optical microscopy. **b** Fluorescence image of Alexa Fluor. **c** Fluorescence image of Texas Red.

images of individual probes are shown in Fig. 3b and c. While a small amount of each probe may have flowed upward around the cannulae, most flow was into the gel, and the two dyes are located in nearly hemispheric regions, indicating substantial nonoverlap of the flows. Close inspection reveals, however, that the Texas Red moves a little farther, and it "invades" the region that is predominantly Alexa Fluor. These observations are most likely due to diffusion, which will be greater for Texas Red because of its lower molecular weight.

CONCLUDING REMARKS

This paper has focused on the convective aspects of CED and R-CED in the brain. We have argued that, for many situations, both of these modalities can be modeled reasonably well using simple spherically symmetric solutions to the Helmholtz equation, which accounts for pressure and flow fields around single cathethers. While real cathethers may have different shapes, spherical fronts develop away from the catheter. Because the volume of the spherical shells increases as one moves away from the central source, the pressure and flow fields for most of the affected tissue are relatively insensitive to catheter shape, provided boundary conditions such as total flow are properly set. Real-time imaging of CED infusions into primate brains demonstrates that tip dimensions and flow rates of currently used catheters in CED protocols generate initial drug distribution with spherical symmetry in homogeneous brain regions (27).

However, spherical symmetry is lost when the infused volume reaches regions of the brain with different tissue properties, leading to channeling effects and uneven drug profiles. As a result, we must keep in mind that although spherical symmetry is a valid approximation within homogenous tissue regions, anatomical differences in the brain can alter expected drug profiles and concentrations. The model for filtration across capillary walls is based on the classical Starling hypothesis, with hydrostatic and osmotic pressures inside the tissue assumed to be volume-averaged field variables. A more recent interpretation of transcapillary wall filtration suggests a more complex picture, however, with concentration polarization of osmolytes adjacent to the endothelial glycocalyx affecting osmotic flow (28). These effects may alter the precise pressure and flow distributions in tissue, but they are unlikely to alter the qualitative behavior.

Although convection through tissue and filtration of fluid across capillaries have been the main emphasis of this paper, transport of drug by diffusion and by solvent drag across capillary walls should be incorporated into more complete descriptions (19–21). As suggested by the phantom experiment, diffusion plays a noticeable but secondary role in distribution of drug. Its effect is expected to be most pronounced in regions where fluid flow is slow (low Peclet number), i.e. away from the catheter, provided drug has not been degraded or removed before reaching those regions.

We have also demonstrated the effect of dual catheters in shaping flow fields and argued that by this means one might steer chemotherapy out of regions of the brain where toxic side effects could occur. Of course, one might consider the effects of multiple catheters in generating drug delivery patterns, subject to surgical constraints. Diffusion may blur the boundaries between flow fields derived from neighboring catheters, however, as illustrated in Fig. 3.

In addition to drug localization, drug patterning by multiple catheters could be useful when drug should be distributed through an entire brain region while sparing critical tissues. This could be accomplished by infusing a non-toxic saline solution into the critical area while simultaneously infusing the drug into the larger regional space.

In order to enable such combination therapies, it will be necessary to know the tissue properties in advance of pattern planning or to use real-time imaging (9,27,29) such that the infusion flow rates could be altered based on the distribution of the ongoing infusion.

We conclude by suggesting further strategies which use CED and R-CED. In one example, a rapidly eliminated blood-brain-barrier-permeable drug could be administered systemically, and a saline solution could be infused into the tumor. The pressure of the saline infusion would reduce drug extravasation into the tumor but would have no such effect in normal tissue. Potential applications include the infusion of radio- or cryoprotectants (30), whereby protectant would accumulate in normal tissue, but tumor would remain susceptible to radiation or cryo therapies.

Parameters governing transport in the brain may be susceptible to manipulation, allowing for alteration in drug

distribution. For example, interstitial hydraulic conductivity might be altered using enzymes such as hyaluronidase to degrade the extracellular matrix (31). Capillary permeability, on the other hand, might be altered by angiogenesis regulators such as VEGF. Such alterations, in addition to changing the region of influence of a catheter, might alter the pressure requirements on catheters to establish a desired drug distribution.

ACKNOWLEDGMENTS

We thank E. Dy for assistance with experiments. This work was carried out with funding provided by NIH R01 CA107268-01. JPMM is a recipient of the NIGMS predoctoral fellowship, supported by the NIGMS-IMSD grant (R25-GM56847). GHH was a recipient of a predoctoral fellowship from the Whitaker Foundation. RAS acknowledges the University of Minnesota for granting a sabbatical which permitted his participation in this work.

REFERENCES

1. Tunggal JK, Cowan DS, Shaikh H, Tannock IF. Penetration of anticancer drugs through solid tissue: a factor that limits the effectiveness of chemotherapy for solid tumors. Clin Cancer Res. 1999;5(6):1583–6.
2. Groothuis DR, Benalcazar H, Allen CV, Wise RM, Dills C, Dobrescu C, *et al.* Comparison of cytosine arabinoside delivery to rat brain by intravenous, intrathecal, intraventricular and intraparenchymal routes of administration. Brain Res. 2000;856(1–2):281–90.
3. Huynh GH, Deen DF, Szoka Jr FC. Barriers to carrier mediated drug and gene delivery to brain tumors. J Control Release. 2006;110(2):236–59.
4. Groothuis DR, Vavra MW, Schlageter KE, Kang EW, Itskovich AC, Hertzler S, *et al.* Efflux of drugs and solutes from brain: the interactive roles of diffusional transcapillary transport, bulk flow and capillary transporters. J Cereb Blood Flow Metab. 2007;27(1):43–56.
5. Chen MY, Lonser RR, Morrison PF, Governale LS, Oldfield EH. Variables affecting convection-enhanced delivery to the striatum: a systematic examination of rate of infusion, cannula size, infusate concentration, and tissue-cannula sealing time. J Neurosurg. 1999;90(2):315–20.
6. Lopez KA, Waziri AE, Canoll PD, Bruce JN. Convection-enhanced delivery in the treatment of malignant glioma. Neurol Res. 2006;28(5):542–8.
7. Hall WA, Rustamzadeh E, Asher AL. Convection-enhanced delivery in clinical trials. Neurosurg Focus. 2003;14(2):E2.
8. Raghavan R, Brady ML, Rodriguez-Ponce MI, Hartlep A, Pedain C, Sampson JH. Convection-enhanced delivery of therapeutics for brain disease, and its optimization. Neurosurg Focus. 2006;20(4):E12.
9. Voges J, Reszka R, Gossmann A, Dittmar C, Richter R, Garlip G, *et al.* Imaging-guided convection-enhanced delivery and gene therapy of glioblastoma. Ann Neurol. 2003;54(4):479–87.
10. Bobo RH, Laske DW, Akbasak A, Morrison PF, Dedrick RL, Oldfield EH. Convection-enhanced delivery of macromolecules in the brain. Proc Natl Acad Sci USA. 1994;91(6):2076–80.
11. Krauze MT, Forsayeth J, Park JW, Bankiewicz KS. Real-time imaging and quantification of brain delivery of liposomes. Pharm Res. 2006;23(11):2493–504.
12. MacKay JA, Deen DF, Szoka Jr FC. Distribution in brain of liposomes after convection enhanced delivery; modulation by particle charge, particle diameter, and presence of steric coating. Brain Res. 2005;1035(2):139–53.
13. DiResta GR, Lee J, Healey JH, Levchenko A, Larson SM, Arbit E. "Artificial lymphatic system": a new approach to reduce interstitial hypertension and increase blood flow, pH and pO2 in solid tumors. Ann Biomed Eng. 2000;28(5):543–55.
14. Huynh GH, Ozawa T, Deen DF, Szoka Jr FC. Retro-convection enhanced delivery to increase blood to brain transfer of macromolecules. Brain Res. 2007;1128(1):181–90.
15. Baxter LT, Jain RK. Transport of fluid and macromolecules in tumors. I. Role of interstitial pressure and convection. Microvasc Res. 1989;37(1):77–104.
16. Kalyanasundaram S, Calhoun VD, Leong KW. A finite element model for predicting the distribution of drugs delivered intracranially to the brain. Am J Physiol. 1997;273(5 Pt 2):R1810–21.
17. Basser PJ. Interstitial pressure, volume, and flow during infusion into brain tissue. Microvasc Res. 1992;44(2):143–65.
18. Levin VA, Patlak CS, Landahl HD. Heuristic modeling of drug delivery to malignant brain tumors. J Pharmacokinet Biopharm. 1980;8(3):257–96.
19. Morrison PF, Laske DW, Bobo H, Oldfield EH, Dedrick RL. High-flow microinfusion: tissue penetration and pharmacodynamics. Am J Physiol. 1994;266(1 Pt 2):R292–305.
20. Smith JH, Humphrey JA. Interstitial transport and transvascular fluid exchange during infusion into brain and tumor tissue. Microvasc Res. 2007;73(1):58–73.
21. Wang P, Olbricht WL. Retro-convection enhanced drug delivery: a computational study. Ann Biomed Eng. 2010;38(8):2512–9.
22. Verwey EJW, Overbeek JThG. Theory of the stability of lyophobic colloids. Mineola: Dover; 2000.
23. Gueron M, Weisbuch G. Polyelectrolyte theory.I.Counterion accumulation, site-binding and their insensitivity to polyelectrolyte shape in solutions containing finite salt concentrations. Biopolymers 1980;19:353–83.
24. Saito R, Bringas JR, McKnight TR, Wendland MF, Mamot C, Drummond DC, *et al.* Distribution of liposomes into brain and rat brain tumor models by convection-enhanced delivery monitored with magnetic resonance imaging. Cancer Res. 2004;64(7):2572–9.
25. Mamot C, Nguyen JB, Pourdehnad M, Hadaczek P, Saito R, Bringas JR, *et al.* Extensive distribution of liposomes in rodent brains and brain tumors following convection-enhanced delivery. J Neurooncol. 2004;68(1):1–9.
26. Krauze MT, Saito R, Noble C, Tamas M, Bringas J, Park JW, *et al.* Reflux-free cannula for convection-enhanced high-speed delivery of therapeutic agents. J Neurosurg. 2005;103(5):923–9.
27. Gimenez F, Krauze MT, Valles F, Hadaczek P, Bringas J, Sharma N, et al. Image-guided convection-enhanced delivery of GDNF protein into monkey putamen. Neuroimage 2010. In press.

28. Hu X, Weinbaum S. A new view of starling's hypothesis at the microstructural level. Microvasc Res. 1999;58:281–304.
29. Saito R, Krauze MT, Bringas JR, Noble C, McKnight TR, Jackson P, *et al.* Gadolinium-loaded liposomes allow for real-time magnetic resonance imaging of convection-enhanced delivery in the primate brain. Exp Neurol. 2005;196(2):381–9.
30. Levi MS, Brimble MA. A review of neuroprotective agents. Curr Med Chem. 2004;11(18):2383–97.
31. Neeves KB, Sawyer AJ, Foley CP, Saltzman WM, Olbricht WL. Dilation and degradation of the brain extracellular matrix enhances penetration of infused polymer nanoparticles. Brain Res. 2007;1180(14):121–32.